# Structural Analyses of Intergrowth and Stacking Fault in Cage-Type Mesoporous Crystals

Yasuhiro Sakamoto,*[,†,‡] Lu Han,[†,§] Shunai Che,*[,§] and Osamu Terasaki[†,‡]

*Structural Chemistry, Arrhenius Laboratory, Stockholm University, SE-10691 Stockholm, Sweden, Berzelii Center EXSELENT, SE-10691, Sweden, and School of Chemistry and Chemical Technology, State Key Laboratory of Composite Materials, Shanghai Jiao Tong University, 800 Dongchuan Road, Shanghai 200240, China*

*Received August 7, 2008. Revised Manuscript Received November 4, 2008*

A mixture of Gemini cationic surfactant, costructure directing agent (CSDA) with carboxylate group, and silica oligomer leads to the formation of cage-type mesoporous crystals, and the system changes the structure from $Fm\bar{3}m$ (or $P6_3/mmc$) type to $Fd\bar{3}m$ type with an increasing amount of additive (HCl). Here we have investigated the $Fm\bar{3}m-Fd\bar{3}m$ type intergrowth and new type stacking fault observed in the intermediate phase using transmission electron microscopy (TEM) and proposed a layer-by-layer growth mechanism. In order to describe the structures, four types of polyhedra for the tetrahedrally close-packed structures are introduced. In the intergrowth, the structure changes the packing of spherical micelles between the $Fm\bar{3}m$ (or $P6_3/mmc$) and $Fd\bar{3}m$ structures depending on the pH. The results can be explained by the change between a hard sphere characteristic (*perfect* sphere) in the $Fm\bar{3}m$ structure and a soft sphere characteristic (polyhedron) in the $Fd\bar{3}m$ structure. The stacking fault in the $Fd\bar{3}m$ structure can be explained by new arrangement of two polyhedra, the 14- and 15-hedron.

## 1. Introduction

Since the first silica mesoporous crystals were reported in early 1990s,[1−4] a variety of ordered structures have been discovered such as bicontinuous, cylindrical, and cage-type. There are several cage-type structures observed, for example, cubic $Im\bar{3}m$ (SBA-16,[5,6] FDU-1[7]), cubic $Fm\bar{3}m$ (SBA-12,[5,8] KIT-5,[9] FDU-12[10]), cubic $Pm\bar{3}n$ (SBA-1,[6,11] SBA-6[6,12]), cubic $Fd\bar{3}m$ (FDU-2,[13] AMS-8[14,15]), hexagonal $P6_3/mmc$ (SBA-2,[12] SBA-11), orthorhombic $Pmmm$ (FDU-13[16]), tetragonal $P4/mmm$ (FDU-11[16]), and tetragonal $P4_2/mnm$ (AMS-9[17]). They can be classified into two types based on the results of three-dimensional (3D) reconstruction by the electron crystallography method.[6,8,15,17] One has a single type of spherical cage such as $Im\bar{3}m$, $Fm\bar{3}m$, and $P6_3/mmc$ structures. The other has several types of spherical cages, typically two, such as $Pm\bar{3}n$ and $Fd\bar{3}m$ structures. The $P4_2/mnm$ structure is also considered as a cage-type structure with three types of cages. All these structures are made up of spherical micelles of block copolymer, cationic surfactant, or anionic surfactant in the mixture with silica oligomer.

In general, micellar types, such as bilayer, cylindrical, and spherical, are simply described by a surfactant packing parameter, $g = V/a_0l$, which is a function of the total volume of the surfactant chains $V$, the effective headgroup area of the surfactant $a_0$, and the kinetic surfactant tail length $l$.[18−21] Based on this scheme, bilayer, cylindrical, and spherical have

* Corresponding authors. E-mail: yasuhiro@struc.su.se, tel: +46-8-16-2382, fax: +46-8-16-3118 (Y.S.); chesa@sjtu.edu.cn, tel: +86-21-5474-2852, fax: +86-21-5474-1297 (S.C.).
† Stockholm University.
‡ Berzelii Center EXSELENT.
§ Shanghai Jiao Tong University.

(1) Yanagisawa, T.; Shimizu, T.; Kuroda, K.; Kato, C. *Bull. Chem. Soc. Jpn.* **1990**, *63*, 988–992.
(2) Kresge, C. T.; Leonowicz, M. E.; Roth, W. J.; Vartuli, J. C.; Beck, J. S. *Nature* **1992**, *359*, 710–712.
(3) Beck, J. S.; Vartuli, J. C.; Roth, W. J.; Leonowicz, M. E.; Kresge, C. T.; Schmitt, K. D.; Chu, C. T. W.; Olson, D. H.; Sheppard, E. W.; Mccullen, S. B.; Higgins, J. B.; Schlenker, J. L. *J. Am. Chem. Soc.* **1992**, *114*, 10834–10843.
(4) Inagaki, S.; Fukushima, Y.; Kuroda, K. *J. Chem. Soc., Chem. Commun.* **1993**, 680–682.
(5) Zhao, D. Y.; Huo, Q. S.; Feng, J. L.; Chmelka, B. F.; Stucky, G. D. *J. Am. Chem. Soc.* **1998**, *120*, 6024–6036.
(6) Sakamoto, Y.; Kaneda, M.; Terasaki, O.; Zhao, D. Y.; Kim, J. M.; Stucky, G.; Shim, H. J.; Ryoo, R. *Nature* **2000**, *408*, 449–453.
(7) Yu, C. Z.; Yu, Y. H.; Zhao, D. Y. *Chem. Commun.* **2000**, 575–576.
(8) Sakamoto, Y.; Diaz, I.; Terasaki, O.; Zhao, D. Y.; Perez-Pariente, J.; Kim, J. M.; Stucky, G. D. *J. Phys. Chem. B* **2002**, *106*, 3118–3123.
(9) Kleitz, F.; Liu, D. N.; Anilkumar, G. M.; Park, I. S.; Solovyov, L. A.; Shmakov, A. N.; Ryoo, R. *J. Phys. Chem. B* **2003**, *107*, 14296–14300.
(10) Fan, J.; Yu, C. Z.; Gao, T.; Lei, J.; Tian, B. Z.; Wang, L. M.; Luo, Q.; Tu, B.; Zhou, W. Z.; Zhao, D. Y. *Angew. Chem., Int. Ed.* **2003**, *42*, 3146–3150.
(11) Huo, Q. S.; Margolese, D. I.; Ciesla, U.; Feng, P. Y.; Gier, T. E.; Sieger, P.; Leon, R.; Petroff, P. M.; Schuth, F.; Stucky, G. D. *Nature* **1994**, *368*, 317–321.
(12) Huo, Q. S.; Leon, R.; Petroff, P. M.; Stucky, G. D. *Science* **1995**, *268*, 1324–1327.
(13) Shen, S. D.; Li, Y. Q.; Zhang, Z. D.; Fan, J.; Tu, B.; Zhou, W. Z.; Zhao, D. Y. *Chem. Commun.* **2002**, 2212–2213.
(14) Garcia-Bennett, A. E.; Terasaki, O.; Che, S.; Tatsumi, T. *Chem. Mater.* **2004**, *16*, 813–821.
(15) Garcia-Bennett, A. E.; Miyasaka, K.; Terasaki, O.; Che, S. *Chem. Mater.* **2004**, *16*, 3597–3605.
(16) Shen, S. D.; Garcia-Bennett, A. E.; Liu, Z.; Lu, Q. Y.; Shi, Y. F.; Yan, Y.; Yu, C. Z.; Liu, W. C.; Cai, Y.; Terasaki, O.; Zhao, D. Y. *J. Am. Chem. Soc.* **2005**, *127*, 6780–6787.
(17) Garcia-Bennett, A. E.; Kupferschmidt, N.; Sakamoto, Y.; Che, S.; Terasaki, O. *Angew. Chem., Int. Ed.* **2005**, *44*, 5317–5322.
(18) Israelachvili, J. N.; Mitchell, D. J.; Ninham, B. W. *J. Chem. Soc., Faraday Trans. 2* **1976**, *72*, 1525–1568.
(19) Huo, Q. S.; Margolese, D. I.; Stucky, G. D. *Chem. Mater.* **1996**, *8*, 1147–1160.
(20) Hyde, S. T. *J. Phys. (Paris)* **1990**, *51*, C7209–C7228.
(21) Hyde, S. T. Identification of lyotropic liquid crystalline mesophases. In *Handbook of Applied Surface and Colloid Chemistry*; Holmberg, K., Ed.; John Wiley & Sons: Chichester, 2001; pp 299−332.

10.1021/cm802162r CCC: $40.75 
Published on Web 12/29/2008

the $g$-value in the range of $1/2 < g \leq 1$, $1/3 < g \leq 1/2$, and $g = 1/3$, respectively. With decreasing the packing parameter, the meso-structure changes from lamellar to cylindrical two-dimensional (2D) hexagonal through bicontinuous cubic, and finally cage-type cubic and tetragonal structures appear. In other words, the surface curvature of the micelle increases toward spherical micelles. This packing parameter describes well the shape of the surfactant micelle itself. However, the mechanism of the micellar packing cannot be described well from the viewpoint of the packing parameter. It is relatively easier to understand the case of cubic close-packed (ccp) and hexagonal close-packed (hcp) structures typified by SBA-12 and SBA-2 with the densest packing of spherical micelles. On the other hand, the bimodal spherical micelle structures, for example, SBA-1 and AMS-8, make it elusive to understand how their structures are stabilized and energetically favorable. In all these cases, the structural relationship and mechanism of each cage-type structure are still not clear and needs to be discussed based on not only the packing parameter but also the characteristics of the micelles and their interactions in the silica−surfactant−water system.

*Fm*$\bar{3}$*m* silica mesoporous crystal has a ccp arrangement of the single type of spherical micelle such as SBA-12. It is typically made from block copolymer, for example, F127, under acidic conditions. In general, the ccp structure is well-known as the structure having the highest packing density of *perfect* spheres, 0.74. The structural analogue, the hcp structure with space group $P6_3/mmc$, also has the same packing density and easily makes an intergrowth with the ccp structure. The ccp structure can be described as *a b c* stacking of hexagonal close-packed layers of hard spheres along $\langle 111 \rangle_c$ direction, and the hcp structure is also described as *a b* stacking of the layers along $[001]_h$ direction.

On the other hand, multimodal silica mesoporous crystals can be described by a tetrahedrally close-packed (tcp) structure. In this structure, the spherical micelle makes an interface with the next micelles and becomes a polyhedron instead of the *perfect* sphere. Figure 1 shows four types of polyhedra, which construct tcp structures. Those four polyhedra are the duals of Frank-Kasper polyhedra, introduced for intermetallic compounds by Frank and Kasper.[22,23] All polyhedra have 12 pentagonal faces like dodecahedron (12-hedron), and other polyhedra have in addition two, three, or four hexagonal faces which are not next each other (14-, 15-, and 16-hedron, respectively).

The *Pm*$\bar{3}$*n* structure (SBA-1) as shown in Figure 2a consists of four 12-hedra arranged in bcc (Wyckoff 2*a* site), and six 14-hedra form three sets of interlocking columns (6*c* site). In 1994 Weaire and Phelan suggested the relaxed version of the *Pm*$\bar{3}$*n* structure with slightly curved edges and faces as a counter-example to Kelvin's conjecture[24] in which Kelvin proposed the structure having a minimum surface area with uniform partition more than 100 years ago, in 1887.[25,26] Furthermore, the *Fd*$\bar{3}$*m* structure (AMS-8) as shown in Figure 2b consists of sixteen 12-hedra and eight 16-hedra in the unit cell. The eight 16-hedra are arranged in the diamond structure (8*b* site) and sixteen 12-hedra are located between 16-hedra (16*c* site). According to a system of symbols for nets, these two structures are categorized as "mep" and "mtn" structures, respectively.[27] In the tcp-type mesoporous crystals, both surfactant micelle (or cage) and silica wall occupy each polyhedron as show in Figure 2c. The *Fd*$\bar{3}$*m* structure can be described as a stacking of two kinds of layers made of these two polyhedra along the $[111]_c$ direction. One of the layers has only 12-hedra arranged in the Kagomé net (Figure 3a), termed layer *A* (or layer *B* or *C*). The other has 12- and 16-hedra as shown in Figure 3b, termed layer α (or layer *β*,

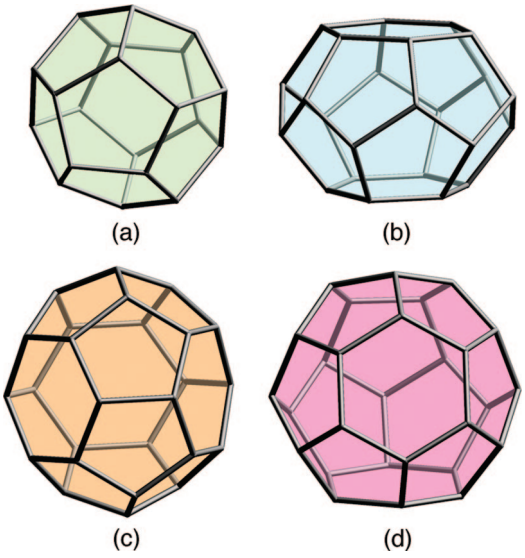


**Figure 1.** Schematic drawings of four types of polyhedra, which make up tetrahedrally close-packed structures. 12-hedron ($5^{12}$-hedron) (a), 14-hedron ($5^{12}6^2$-hedron) (b), 15-hedron ($5^{12}6^3$-hedron) (c), and 16-hedron ($5^{12}6^4$-hedron) (d).

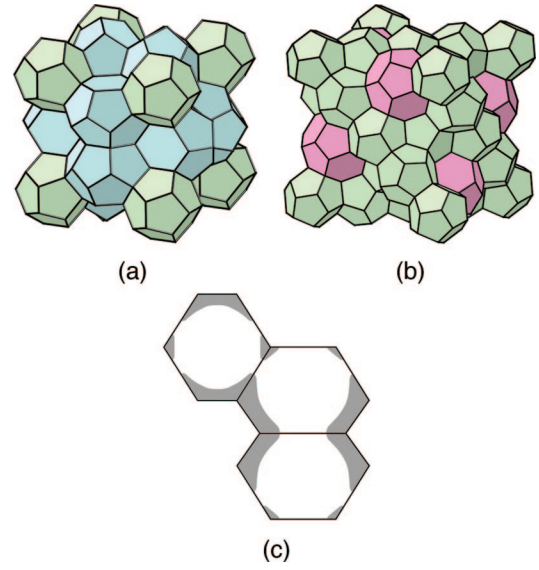


**Figure 2.** Representations of the *Pm*$\bar{3}$*n* structure (a) and the *Fd*$\bar{3}$*m* structure (b). The polyhedra occupied by cage (white) and silica wall (gray) (c). Cages can be connected to each other through a window.

(22) Frank, F. C.; Kasper, J. S. *Acta Crystallogr.* **1958**, *11*, 184–190.
(23) Frank, F. C.; Kasper, J. S. *Acta Crystallogr.* **1959**, *12*, 483–499.
(24) Weaire, D.; Phelan, R. *Philos. Mag. Lett.* **1994**, *69*, 107–110.
(25) Thomson, W. *Philos. Mag.* **1887**, *24*, 503–514.
(26) Weaire, D. *The Kelvin Problem: Foam Structures of Minimal Surface Area*; Taylor & Francis: London, 1996.
(27) Friedrichs, O. D.; O'Keeffe, M.; Yaghi, O. M. *Acta Crystallogr., Sect. A* **2003**, *59*, 22–27 (see also the *Reticular Chemistry Structural Resource*, http:/rcsr.anu.edu.au).

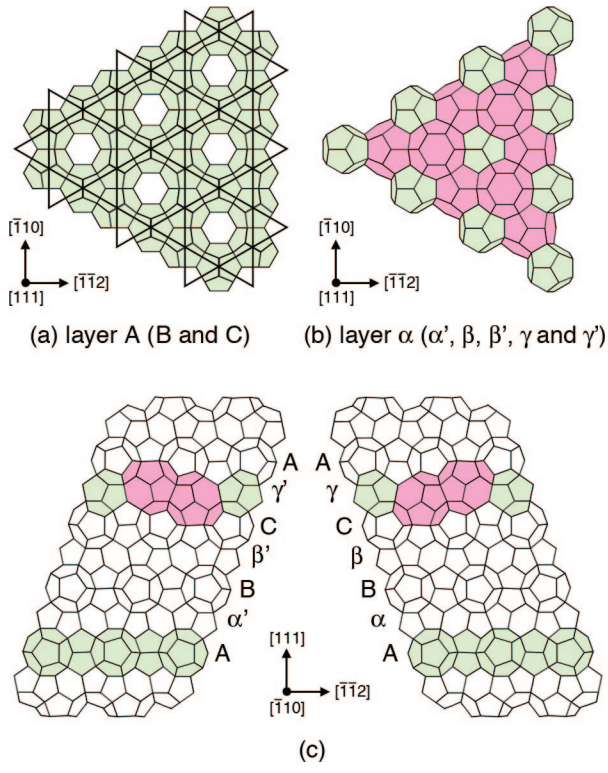


**Figure 3.** Schematic drawings of the $Fd\bar{3}m$ structure. Layer *A* which consists of only 12-hedra arranged in Kagomé net (a) and layer α which consists of 12- and 16-hedra (b). Stacking sequence of both layers along [111] direction (c).

$\beta'$, $\gamma'$, or $\gamma$). Figure 3c shows the stacking sequence of the $Fd\bar{3}m$ structure made by these two types of layers, layer *A* and layer α, where layer α and layer α′ are related each other by mirror plane. The same goes for layer $\beta$ and layer $\beta'$ and layer $\gamma$ and layer $\gamma'$.

In the carboxylic group functionalized mesoporous silicas (CFMS) using cationic surfactant, the meso-structure changes from the $Fm\bar{3}m$ structure to $Fd\bar{3}m$ structure with increasing the amount of HCl.[28] In the intermediate phase, the intergrowth of these two structures has been directly observed using transmission electron microscopy (TEM) with a new type of stacking fault. Defects of mesoporous crystals can be more diverse than crystalline solids because the meso-structure before completion of silica condensation is more flexible and the energy required for stabilizing defects is far less than in crystalline solids, thereby making the formation of defects more likely.[29,30] The defect in the solid affects the properties of materials, and it is of importance to control the defect in terms of crystal nucleation, growth, bulk and surface catalytic reactivity, and diffusion properties. It is also crucial to achieve a proper internal structure and morphological features without defects for many applications. TEM is the only technique capable of giving direct information of the local structure in meso-scale.[31−34] Furthermore, 3D structures of mesoporous crystals can be reconstructed using the electron crystallography or tomography methods.[6,8,15,17,35−39] Here we have investigated the detail structure of the intergrowth and stacking fault and proposed a structural model based on the characteristics of silica−CSDA−surfactant micelles in water.

## 2. Experimental Section

**Preparation of CFMS.** Reagents and materials for preparation of CFMS and surfactant preparation are described in Supporting Information S1. A typical synthesis route by using TEOS as precursor and carboxyethylsilanetriol sodium salt (CES) as CSDA was as follows. A total of 1.40 g of Gemini surfactant was dissolved in 9.00 g of deionized water followed by *x* g of HCl ($x = 0.8-2.4$), then 0.39 g of CES was added together with 0.78 g of TEOS, and the mixture was stirred for 2 h at room temperature. The final composition is $C_{18-3-1}$:2CSS:*x*HCl:15TEOS:2000$H_2O$ ($x = 0.8-2.4$). The mixture was then transferred to a Teflon bottle and heated at 373 K for 2 days. The surfactant was removed from the as-synthesized material by calcination at 550 °C for 6 h.

**Transmission Electron Microscopy.** For TEM observation, the sample was crushed in an agate mortar, dispersed in ethanol, and dropped on a carbon thin film on a Cu grid. High-resolution TEM (HRTEM) was performed with a JEOL JEM-3010 microscope operating at 300 kV (Cs = 0.6 mm, point resolution 1.7 Å). Images were recorded with a CCD camera (MultiScan model 794, Gatan, 1024 × 1024 pixels, pixel size 24 $\mu$m) at 50 000−80 000 times magnification under low-dose conditions. TEM image simulations of the idealized mesoporous structures were performed using dedicated software of MesoPoreImage.[40] The MesoPoreImage provides the image calculated from a 3D continuum model of mesoporous crystal structure. In order to adjust the image contrast of the simulated to that of the observed, a parameter representing surface roughness on the pore surface was introduced.

## 3. Results and Discussion

**3.1. $Fm\bar{3}m$ Structure and $Fd\bar{3}m$ Structure.** With increasing the amount of HCl in the synthesis conditions, structural change from the $Fm\bar{3}m$ (HCl = 0.8−1.9) to $Fd\bar{3}m$ (HCl = 2.1−2.4) structures occurs; see powder XRD pattern in Supporting Information S2. Figure 4 shows HRTEM images of $Fm\bar{3}m$ (HCl = 1.9) and $Fd\bar{3}m$ (HCl = 2.1) structures taken along the $[\bar{1}10]_c$ direction. Figure 4a shows intergrowth of ccp ($Fm\bar{3}m$) and hcp ($P6_3/mmc$) structures, where both *a b c* (for ccp) and *a b* (for hcp) stacking sequences are observed. The stacking faults make streaks along the [111] stacking direction in the Fourier diffractogram (marked with arrows). Figure 4b shows the $Fd\bar{3}m$ structure with several stacking faults. Cubic stacking (e.g., *A* α *B* $\beta$ *C* $\gamma$) and hexagonal stacking (e.g., *B* $\beta$

(28) Han, L.; Sakamoto, Y.; Terasaki, O.; Li, Y.; Che, S. *J. Mater. Chem.* **2007**, *17*, 1216–1221.
(29) Yang, H.; Ozin, G. A.; Kresge, C. T. *Adv. Mater.* **1998**, *10*, 883–887.
(30) Hillhouse, H. W.; van Egmond, J. W.; Tsapatsis, M.; Hanson, J. C.; Larese, J. Z. *Chem. Mater.* **2000**, *12*, 2888–2893.
(31) Kamiya, S.; Tanaka, H.; Che, S.; Tatsumi, T.; Terasaki, O. *Solid State Sci.* **2003**, *5*, 197–204.
(32) Diaz, I.; Perez-Pariente, J.; Terasaki, O. *J. Mater. Chem.* **2004**, *14*, 48–53.
(33) Garcia-Bennett, A. E.; Lund, K.; Terasaki, O. *Angew. Chem., Int. Ed.* **2006**, *45*, 2434–2438.
(34) Han, L.; Sakamoto, Y.; Che, S.; Terasaki, O. *Chem.—Eur. J.*
(35) Carlsson, A.; Kaneda, M.; Sakamoto, Y.; Terasaki, O.; Ryoo, R.; Joo, S. H. *J. Electron Microsc.* **1999**, *48*, 795–798.
(36) Kaneda, M.; Tsubakiyama, T.; Carlsson, A.; Sakamoto, Y.; Ohsuna, T.; Terasaki, O.; Joo, S. H.; Ryoo, R. *J. Phys. Chem. B* **2002**, *106*, 1256–1266.
(37) Sakamoto, Y.; Kim, T. W.; Ryoo, R.; Terasaki, O. *Angew. Chem., Int. Ed.* **2004**, *43*, 5231–5234.
(38) Gao, C. B.; Sakamoto, Y.; Sakamoto, K.; Terasaki, O.; Che, S. *Angew. Chem., Int. Ed.* **2006**, *45*, 4295–4298.
(39) Yates, T. J. V.; Thomas, J. M.; Fernandez, J. J.; Terasaki, O.; Ryoo, R.; Midgley, P. A. *Chem. Phys. Lett.* **2006**, *418*, 540–543.
(40) Ohsuna, T.; Sakamoto, Y.; Terasaki, O.; Kuroda, K. In preparation.

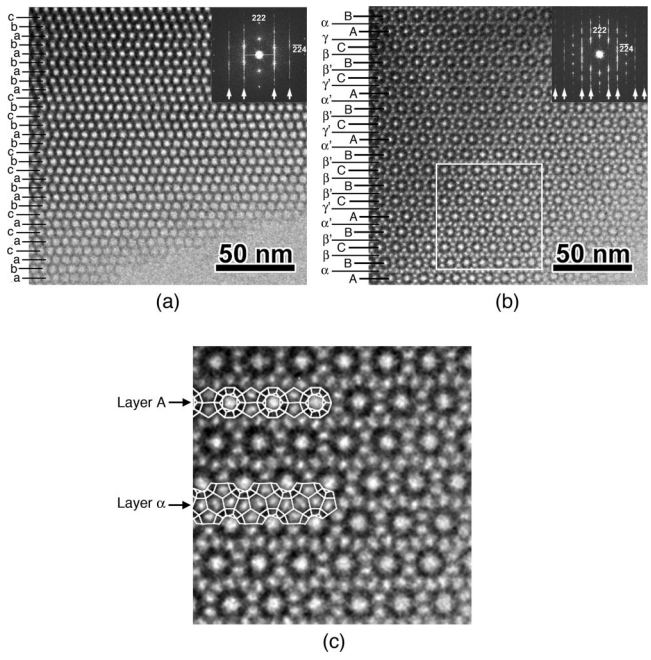


**Figure 4.** HRTEM images and their Fourier diffractograms of the $Fm\bar{3}m$ structure ([$\bar{1}$10] direction) (a) and the $Fd\bar{3}m$ structure ([110] direction) (b) and magnified image of white square region in (b) with the shematic drawings of layer A and layer α (c). The stacking faults make streaks along [111] direction in the Fourier diffractograms as marked with arrows.

*C β′*) are observed. Figure 4c shows a magnified HRTEM image, and two kinds of layers, for example, layer *A* and layer α, are also displayed in the image. The unit cell parameters are $a_{Fm\bar{3}m}$ = 10.1 nm for the $Fm\bar{3}m$ structure and $a_{Fd\bar{3}m}$ = 16.9 nm for the $Fd\bar{3}m$ structure, calculated from their electron diffraction patterns.

**3.2. Intergrowth of $Fm\bar{3}m$ and $Fd\bar{3}m$ Structures.** In the intermediate phase (HCl = 2.0), the intergrowth of the $Fm\bar{3}m$ and $Fd\bar{3}m$ structures is observed (see powder XRD pattern in Supporting Information S2). Figure 5 shows the intergrowth of two successive tilt series (30° between them) from the same area. It is clear from the HRTEM images (Figure 5) and Fourier diffractograms of both domains (Supporting Information S3) that the [$\bar{1}$10] direction of the $Fm\bar{3}m$ structure (top and bottom domains) corresponds with the [$\bar{2}$11] of the $Fd\bar{3}m$ structure (middle domain) with common [111] axis in Figure 5a and the [$\bar{2}$11] of the $Fm\bar{3}m$ structure and the [$\bar{1}$01] of the $Fd\bar{3}m$ structure in Figure 5b as well. From these results, we can conclude that the $Fm\bar{3}m$ structure and the $Fd\bar{3}m$ structure have epitaxial relationship with 30° rotation along common [111] axis. They have a relationship of $a_{Fd\bar{3}m}/a_{Fm\bar{3}m} = \sqrt{3} \approx 1.73$. It is consistent with the unit cell parameters of $a_{Fd\bar{3}m}$ = 16.2 nm ($Fd\bar{3}m$ domain) and $a_{Fm\bar{3}m}$ = 9.3 nm ($Fm\bar{3}m$ domain), that is, $a_{Fd\bar{3}m}/a_{Fm\bar{3}m}$ = 1.74, calculated from their electron diffraction patterns.

Figure 6 shows magnified HRTEM images of the boundary of two structures. Based on the HRTEM images, the intergrowth model from the $Fd\bar{3}m$ structure to the $Fm\bar{3}m$ structure is considered as the following. The structural change may take place on 12-hedron layer (layer *A*) of the $Fd\bar{3}m$ structure. Figure 7 shows the new layer structure (termed layer λ) on the layer *A*. The layer λ consists of two kinds of spheres, where a small sphere occupies the lattice point of the triangular net as shown in orange color, and a large sphere is on the center of hexagon of the Kagomé net as shown in blue. The layer λ results in the base layer (e.g., layer *a*) for the successive $Fm\bar{3}m$ structure. The hexagonal close-packed layer, for example, layer *c* in Figure 6, can be placed on layer λ for the ccp (λ (= *a*) *b c a b c*...) or hcp (λ (= *a*) *b a b*...) structures. TEM images of the boundary are simulated based on the model. A good agreement is observed with HRTEM images as shown in Figure 6. Each cage size for the image simulation is listed in Table 1, where the cages were occupied by the surfactant before calcination. For simplification, all cages were assumed as *perfect* spheres instead of polyhedra, and sphere−sphere overlap was permitted if necessary. In the layer λ, the small sphere has the same size as the 12-hedron of layer *A* and layer α, and the large sphere has the same size as the 16-hedron of layer α. Therefore, two kinds of micelles may keep their size during structural change whereas they change their arrangements and characteristics in the layer λ for the successive hexagonal close-packed layer of the $Fm\bar{3}m$ structure. It is worth noting that the volume of the large sphere (16-hedron) is twice of the small sphere (12-hedron) whereas that of the sphere of the $Fm\bar{3}m$ structure is between the small and large spheres.

**3.3. New Stacking Fault in the $Fd\bar{3}m$ Structure.** Several stacking faults are observed in the $Fd\bar{3}m$ domain as shown in Figure 8a,b. The domain consists of *A C C A B A C C* stacking of 12-hedron layers, where a new stacking sequence (*C C*) is observed. This stacking sequence is not allowed in the $Fd\bar{3}m$ structure and has not been reported in the silica mesoporous system. This new layer between two 12-hedron layers (layer *C*) is termed layer *z*. The full explanation of the $Fd\bar{3}m$ domain in Figure 5 is the following from bottom to top

$$A\gamma'\,\underline{CzC}\gamma A\alpha B\alpha'\,A\gamma'\,\underline{CzC}\gamma\underline{AzA}\gamma'\,C\gamma A$$

Figure 9 shows the new layer *z* with layer *A*, which consists of two types of polyhedra. One is 15-hedron, which has twelve pentagons and three hexagons, and it is arranged in the triangular net. The other is 14-hedron, which has twelve pentagons and two hexagons, and it occupies the center of the triangular net. It leaves us another possibility of the new mesoporous crystal which consists of only layer *z*. It may have a 3D hexagonal structure with *P6/mmm* symmetry. Interestingly, 14-hedron is also one of the constituents for the $Pm\bar{3}n$ and $P4_2/mnm$ structures. Schematic figures of the layers and simulated TEM images of layer *z* are inserted in HRTEM images (Figure 8), and they fit the contrast of the observed image. Each cage size for image simulation is listed in Table 2, where 15-hedron was assumed as spheroid because the simulated image was far from the observed image by using *perfect* spherical shape. Although all the cages have different volumes, the new layer *z* has the same arrangement of two polyhedra as that of two spheres in layer λ as shown in Figure 7. The 15-hedron corresponds with the small sphere of layer λ and the 14-hedron with the large sphere of layer λ.

**3.4. Layer-by-Layer Growth Mechanism of the Hard Sphere $Fm\bar{3}m$ Structure and Soft Sphere $Fd\bar{3}m$ Structure.** We found several types of stacking sequences and new layer structures in the intermediate meso-structure. All structural changes take place on layer *A*, that is, the Kagomé

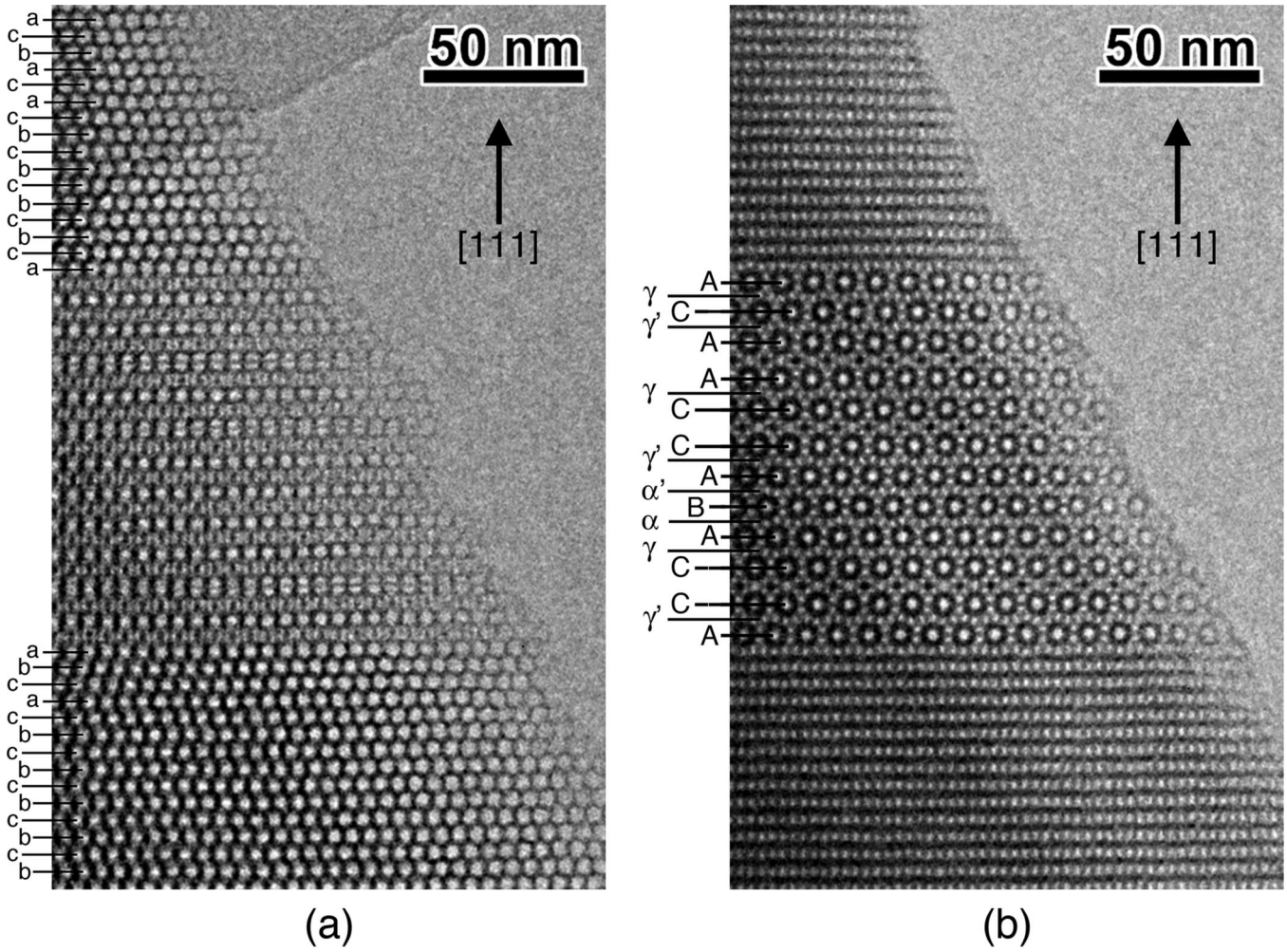


**Figure 5.** HRTEM images of the intergrowth of the $Fm\bar{3}m$ (top and bottom) and $Fd\bar{3}m$ (middle) structures. Each domain is taken along $[\bar{1}10]_{Fm\bar{3}m}$ and $[\bar{2}11]_{Fd\bar{3}m}$ directions (a) and $[\bar{2}11]_{Fm\bar{3}m}$ and $[\bar{1}01]_{Fd\bar{3}m}$ directions (b).

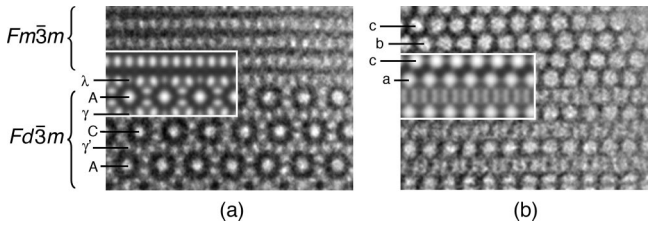


**Figure 6.** Magnified HRTEM images of the intergrowth of the $Fm\bar{3}m$ and $Fd\bar{3}m$ structures with simulated TEM images.

net of 12-hedra, of the $Fd\bar{3}m$ structure through two kinds of intermediate layers (layer $\lambda$ and layer $z$) which control the successive layers. Figure 10 summarizes possible stacking sequences as well as the $Fd\bar{3}m$ sequence. For the further discussion of the growth mechanism, two micellar characteristics, hard sphere and soft sphere, are introduced. In the $Fm\bar{3}m$ structure, a micelle is considered as a hard sphere, which has a packing parameter of 1/3, resulting in the densest packing of uniform hard spheres. On the other hand, in order to attain bimodal micelles for the $Fd\bar{3}m$ structure the micellar size and shape have to be adjustable as a soft sphere during the crystallization, resulting in the polyhedra.

*(i) $Fd\bar{3}m$ Structure (stacking sequence: A α B β C γ or A γ′ C β′ B α′).* When layer *B* is placed after layer *A* with the shift of (2/3, 1/3) unit cell through layer α, this stacking

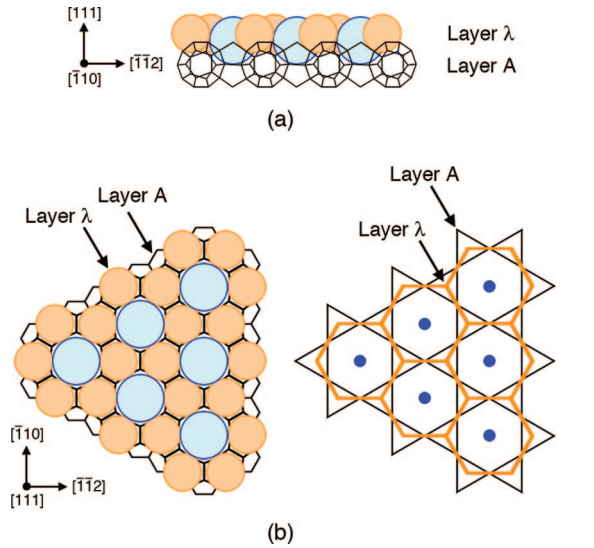


**Figure 7.** Schematic drawings of the boundary layer (layer $\lambda$) on layer *A* along $[\bar{1}10]$ (a) and [111] (b) directions.

sequence, *A* α *B*, results in the $Fd\bar{3}m$ structure. In the layer α structure, the two different cages occupy three unique sites on the layer *A*. One 12-hedron is at one of the triangle sites of the Kagomé net (site A) and one 16-hedron at the other

**Table 1. Cage Type and Cage Size for the Image Simulation of Intergrowth with Relative Volume Ratio**

| cage type | cage size (radius) | relative volume |
|---|---|---|
| small sphere (layer $\lambda$), 12-hedron (layer *A* and layer $\alpha$) | 2.75 nm | 1.00 |
| large sphere (layer $\lambda$), 16-hedron (layer $\alpha$) | 3.50 nm | 2.06 |
| $Fm\bar{3}m$ structure hard sphere (layer *a*) | 3.10 nm | 1.43 |

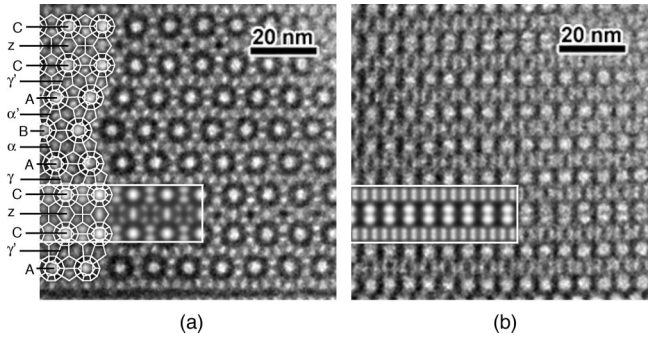


**Figure 8.** Magnified HRTEM images of the $Fd\bar{3}m$ structure with stacking faults taken along [$\bar{1}$10] (a) and [$\bar{2}$11] (b) directions. Simulated TEM images and schematic drawings are inserted.

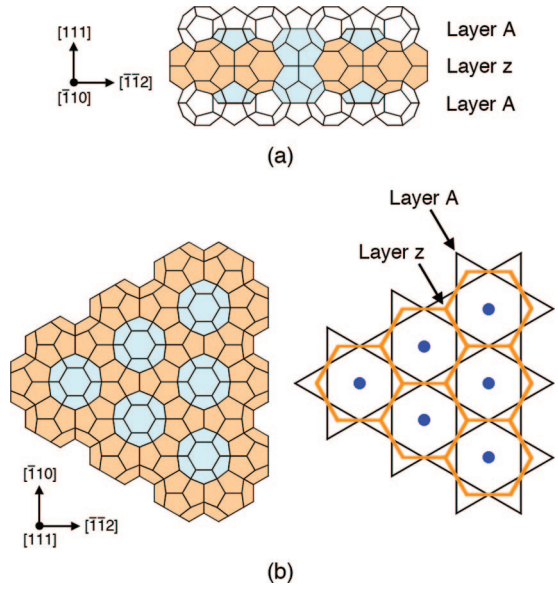


**Figure 9.** Schematic drawing of the layer *z* along [$\bar{1}$10] (a) and [111] (b) directions.

**Table 2. Cage Type and Cage Size for the Image Simulation of Layer *z* with Relative Volume Ratio**

| cage type | cage size (radius) | relative volume |
|---|---|---|
| 12-hedron (layer *A*) | 2.75 nm | 1.00 |
| 14-hedron (layer *z*) | 3.05 nm | 1.36 |
| 15-hedron (layer *z*) *1[a] | $a = b = 3.05$ nm and $c = 3.45$ nm | 1.54 |

[a] *1: Spheroid was assumed.

triangle site (site B). The hexagonal site of the Kagomé net (site C) is occupied by the 16-hedron.

*(ii) New Structure in the $Fm\bar{3}m$ structure (A z A).* When the layer *A* is placed on the top of layer *A* without shift through layer *z*, this stacking sequence (*A z A*) is the new type of layer structure observed in the $Fd\bar{3}m$ domain. 15-hedron is placed at the triangle site of layer *A* (sites A and B) and two connected 14-hedra along stacking direction occupy hexagonal site (site C). The difference between case (i) and (ii) is the difference of the arrangement and size of the polyhedra on the layer *A*.

*(iii) Boundary between the $Fm\bar{3}m$ and $Fm\bar{3}m$ Structures (A λ b).* The hexagonal close-packed layer, layer *b* or layer *c*, is following layer *A* through layer $\lambda$, leading to an intergrowth of the $Fd\bar{3}m$ and $Fm\bar{3}m$ structures. The stacking sequence of the boundary is *A λ b*. The arrangement of the spheres in the layer $\lambda$ is the same as that of the layer *z*, but two spheres of the layer $\lambda$ may have both soft and hard sphere characteristic for the precedent $Fd\bar{3}m$ structure and the successive $Fm\bar{3}m$ structure, respectively. A small sphere occupies the triangle site of layer *A* (site A and B) and a large sphere occupies the hexagonal site (site C).

*(iv) $Fm\bar{3}m$ ($P6_3/mmc$) Structure (a b c or a b).* The $Fm\bar{3}m$ structure consists of the stacking of hexagonal close-packed layers, such as layer *a*. On the top of the $Fm\bar{3}m$ structure, any of the hexagonal close-packed layers can be followed by layer $\lambda$ as a base layer for the $Fd\bar{3}m$ structure.

In this system, the interaction between the negatively charged carboxylate site of CES and the positively charged headgroup of the cationic surfactant can be controlled by the additive HCl.[28] Accordingly the appropriate spherical micellar packing such as $Fm\bar{3}m$ and $Fd\bar{3}m$ structures is constructed, where the main factor of the packing can be the delicate interaction between the micelle/CSDA/silica composites. In the low amount of HCl, the pH of the solution is basic due to the presence of the sodium alcoholate group of the CSDA. As a result, the spherical micelle tends to be a hard sphere and leads to the $Fm\bar{3}m$ structure with the densest packing. On the other hand, addition of HCl makes the solution more neutral. It leads to the possibility for the spherical micelle to be a soft sphere instead of a hard sphere due to the ionization degree of CSDA, where the size and shape of the sphere are variable. Then, the micellar packing may take the tcp structure, that is, the $Fd\bar{3}m$ structure. The intergrowth of the $Fm\bar{3}m$ and $Fd\bar{3}m$ structures in the intermediate phase suggests to us that the ionization degree of carboxylate groups of CSDA varies locally during the crystal growth. This fluctuation leads to the oscillatory growth of both structural types. It is worth noting that Che reported the structural change between $P6_3/mmc$ and $Pm\bar{3}n$ structures, where the meso-structure consists of cationic surfactant and silica source under acidic condition with various acids such as $H_2SO_4$ and HCl.[41,42] It can be the same type of structural change between hard and soft sphere type structures as observed in this system. They discussed the effect of ionic species, in which the meso-structure is controlled by the charge density matching between the surfactant and silicate and the rate of silica condensation caused by counteranion.

With respect to the relative stability of the hard and soft sphere type structures, Ziherl and Kamien proposed that micellar structures are determined by the balance between a

(41) Che, S.; Lim, S. Y.; Kaneda, M.; Yoshitake, H.; Terasaki, O.; Tatsumi, T. *J. Am. Chem. Soc.* **2002**, *124*, 13962–13963.
(42) Che, S.; Li, H. C.; Lim, S.; Sakamoto, Y.; Terasaki, O.; Tatsumi, T. *Chem. Mater.* **2005**, *17*, 4103–4113.

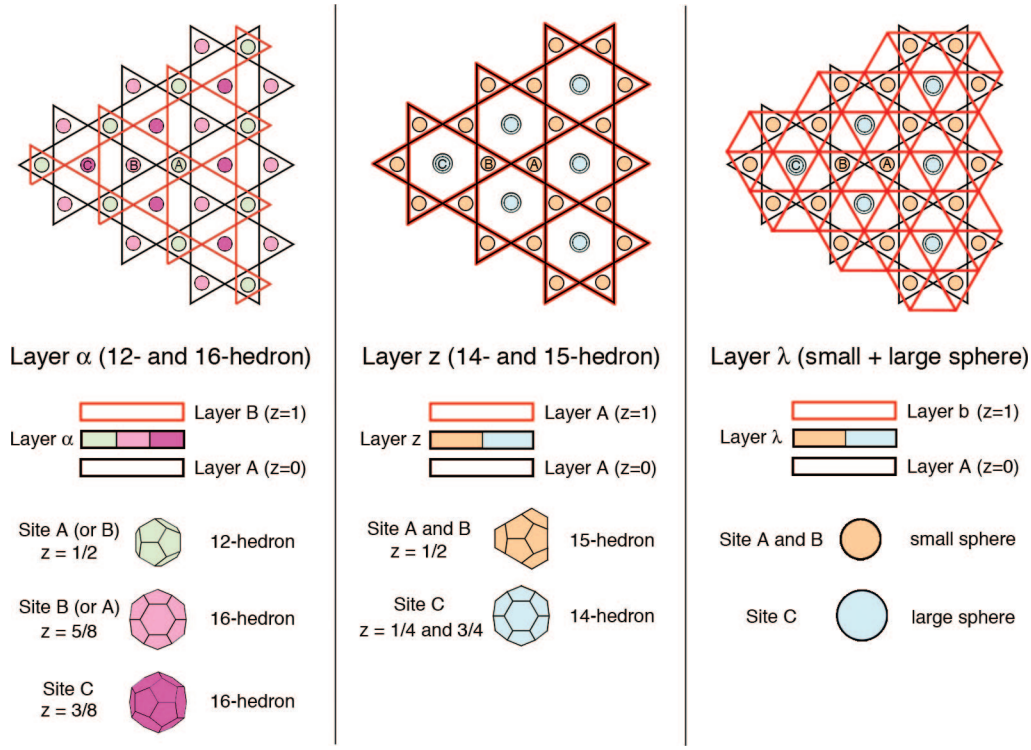


**Figure 10.** Schematic drawings of three possible stacking sequences with layer *A*.

close-packing rule associated with the hard-core interactions and positional entropy, and a minimum-area principle associated with the soft tail and internal entropy of the soft coronas.[43,44] The former leads to the hard sphere type structure and the latter leads to the soft sphere type structure. This principle has been applied to surfactant/water systems[45] and may possibly be applicable to mesoporous silica systems, too. From another perspective, the Weaire−Phelan structure, which is the relaxed version of the $Pm\bar{3}n$ structure and one of the soft sphere type structure, has been considered as the smallest area minimized structure with equal volumes. However, it is obvious that the soft sphere type $Fd\bar{3}m$ structure has two kinds of cages (polyhedra or composites) with different volumes. It means that we have less volume constrains in micelles, that is, unlike foams, micelles of different volumes may be allowed with keeping a minimum-area principle. These two points need to be taken into account in order to discuss the stability of the structures.

## 4. Conclusion

Intergrowth of two typical structures with $Fm\bar{3}m$ (or $P6_3/mmc$) and $Fd\bar{3}m$ symmetries was investigated using TEM. Direct observation by TEM clearly shows the epitaxial relationship between the two cubic structures with 30° rotation along the common [111] axis. The simulated TEM images of the proposed structural model for the boundary of two structures agree very well with the observed ones in both successive tilt angles. In the intergrowth, the structure changes the packing of spherical micelles between the hard sphere packing with the $Fm\bar{3}m$ (or $P6_3/mmc$) structure and the soft sphere packing with the $Fd\bar{3}m$ structure. It may be caused by the slightly different pH conditions in the synthesis solution due to the additive HCl. Furthermore, the new type layer has an arrangement of 14- and 15-hedra and was observed as a planer defect in the $Fd\bar{3}m$ structure. A layer-by-layer crystal growth mechanism together with the local fluctuation in the solution plays an important role for the defect formation. To study the precise size, shape, and surface area of the each sphere will be very important not only to understand these structural changes quantitatively but also to get deep knowledge of how they stabilize their structures and how the synthesis conditions affect their structures. Further studies will focus on these points.

**Acknowledgment.** The authors thank T. Ohsuna for helpful discussion and the software MesoporeImage for the TEM image simulation and I. Díaz and A. E. Garcia-Bennett for many helpful discussions. Y.S. and O.T. thank the Swedish Research Council (VR), Japan Science and Technology Agency (JST), and the Berzelii Center EXSELENT for financial support. S.C. thanks the National Natural Science Foundation of China (Grant Nos. 20425102, 20501015, and 20521140450). TEM studies were performed at the Electron Microscopy Center (EMC) at Stockholm University, which is supported by the Knut and Alice Wallenberg Foundation.

**Supporting Information Available:** Additional experimental details, powder XRD patterns, and Fourier diffractograms (PDF). This material is available free of charge via the Internet at http://pubs.acs.org.

(43) Ziherl, P.; Kamien, R. D. *Phys. Rev. Lett.* **2000**, *85*, 3528–3531.
(44) Ziherl, P.; Kamien, R. D. *J. Phys. Chem. B* **2001**, *105*, 10147–10158.
(45) Imai, M.; Yoshida, I.; Iwaki, T.; Nakaya, K. *J. Chem. Phys.* **2005**, *122*, 044906.

CM802162R